RSC Advances

PAPER

View Article Online
View Journal | View Issue

Cite this: *RSC Adv.*, 2018, **8**, 28684

Hierarchical Co–FeS_2/CoS_2 heterostructures as a superior bifunctional electrocatalyst†

Ka Wang,[a] Weilan Guo,[a] Shancheng Yan,*[a] Haizeng Song[a] and Yi Shi*[bc]

Received 19th June 2018
Accepted 7th August 2018

DOI: 10.1039/c8ra05237a

rsc.li/rsc-advances

The traditional method of preparing hydrogen and oxygen as efficient clean energy sources mainly relies on the use of platinum, palladium, and other precious metals. However, the high cost and low abundance limit wide application of such metals. As such, one challenging issue is the development of low-cost and high-efficiency electrocatalysts for such purposes. In this study, we synthesized Co–FeS_2/CoS_2 heterostructures *via* a hydrothermal method for efficient hydrogen evolution reaction (HER) and oxygen evolution reaction (OER). Benefitting from their unique three-dimensional hierarchical nanostructures, Co-doped FeS_2, and CoS_2 formed heterostructures on Co–FeS_2 petals, which bestowed remarkable electrocatalytic properties upon Co–FeS_2/CoS_2 nanostructures. Co–FeS_2/CoS_2 effectively catalyzed the OER with an overpotential of 278 mV at a current density of 10 mA cm^{-2} in 1 M KOH solution, and also is capable of driving a current density −10 mA cm^{-2} at an overpotential of −103 mV in 0.5 M H_2SO_4 solution. The overpotential of the OER and HER only decreased by 5 mV and 3 mV after 1000 cycles. Our Co–FeS_2/CoS_2 materials may offer a promising alternative to noble metal-based electrocatalysts for water splitting.

1. Introduction

In response to global energy and environmental problems, researchers have made tremendous efforts to explore and develop high-performance and low-cost electrocatalysts for HER and OER to replace platinum, palladium and other precious metals.[1–5] Non-noble metal electrocatalysts such as Fe, Co, Ni, Mo, and their sulfides,[6–8] phosphides[9–12] or their alloys[13–17] have been investigated widely as electrocatalysts over the past decades. Among them, the low-cost, earth-abundant iron sulfide has attracted much attention as an electrocatalytic material due to its excellent catalytic activity.[7,18] However, the catalytic performance of iron sulfide is limited by its low surface area and lack of active sites.[19] If the non-noble metals electrocatalysts are grown on carbon material substrates, doping with homologous elements not only reduces the catalytic resistance but also exposes more active sites.[20–22] Furthermore, the formation of epitaxial heterostructures can regulate the energy barrier between the two interfaces to reduce the catalytic kinetic energy.[23–25]

In this work, we prepared Co–FeS_2/CoS_2 heterostructures electrocatalysts on a carbon cloth (CC) by using sulfur powder and thiourea as sulfur sources and show that they have excellent catalytic performance. The unique 3D hierarchical nanostructures give it a high surface area and the doping of cobalt reduced the kinetic energy barrier of the catalytic reaction of FeS_2. The bumps heterostructures of CoS_2 further exposed more active sites and adjusted the kinetic energy barrier for catalytic reaction at the two interface junctions, which led to the remarkable electrocatalytic properties. The as-synthesized Co–FeS_2/CoS_2 materials has an exceptional overpotential of 278 mV at a current density of 10 mA cm^{-2} in 1 M KOH solution and the Tafel slope is only 73 mV dec^{-1}. The overpotential is −103 mV at a current density of −10 mA cm^{-2} in 0.5 M H_2SO_4 solution, and the Tafel slope is only 56 mV dec^{-1}. In addition, the overpotential of OER and HER only decreased by 5 mV and 3 mV after 1000 cycles. Our Co–FeS_2/CoS_2 materials may be a promising alternative to noble metal-based electrocatalysts for water splitting applications.

2. Experimental section

2.1 Chemicals and materials

WOS1009 carbon cloth (CC) was supplied by CeTech Co., Ltd. $FeSO_4 \cdot 7H_2O$, was purchased from Shanghai Titan Scientific Co., Ltd. CH_3CSNH_2 was purchased from Aladdin Ltd. $Co(NO_3) \cdot 6H_2O$, sulfur power (S), thiourea ($SC(NH_2)_2$), $Na_2S \cdot 9H_2O$, C_2H_5OH, H_2SO_4, and KOH were purchased from Nanjing Chemical Reagent Co., Ltd. Ultrapure water was obtained using a Millipore pure water filter (Millipore Q, USA).

[a]*School of Geography and Biological Information, Nanjing University of Posts and Telecommunications, Nanjing 210023, P. R. China. E-mail: yansc@njupt.edu.cn; Fax: +86-25-85866634; Tel: +86-25-85866635*

[b]*National Laboratory of Solid State Microstructures, Nanjing University, Nanjing 210093, P. R. China. E-mail: yshi@nju.edu.cn*

[c]*Collaborative Innovation Center of Advanced Microstructures, Nanjing University, Nanjing 210093, P. R. China*

† Electronic supplementary information (ESI) available. See DOI: 10.1039/c8ra05237a

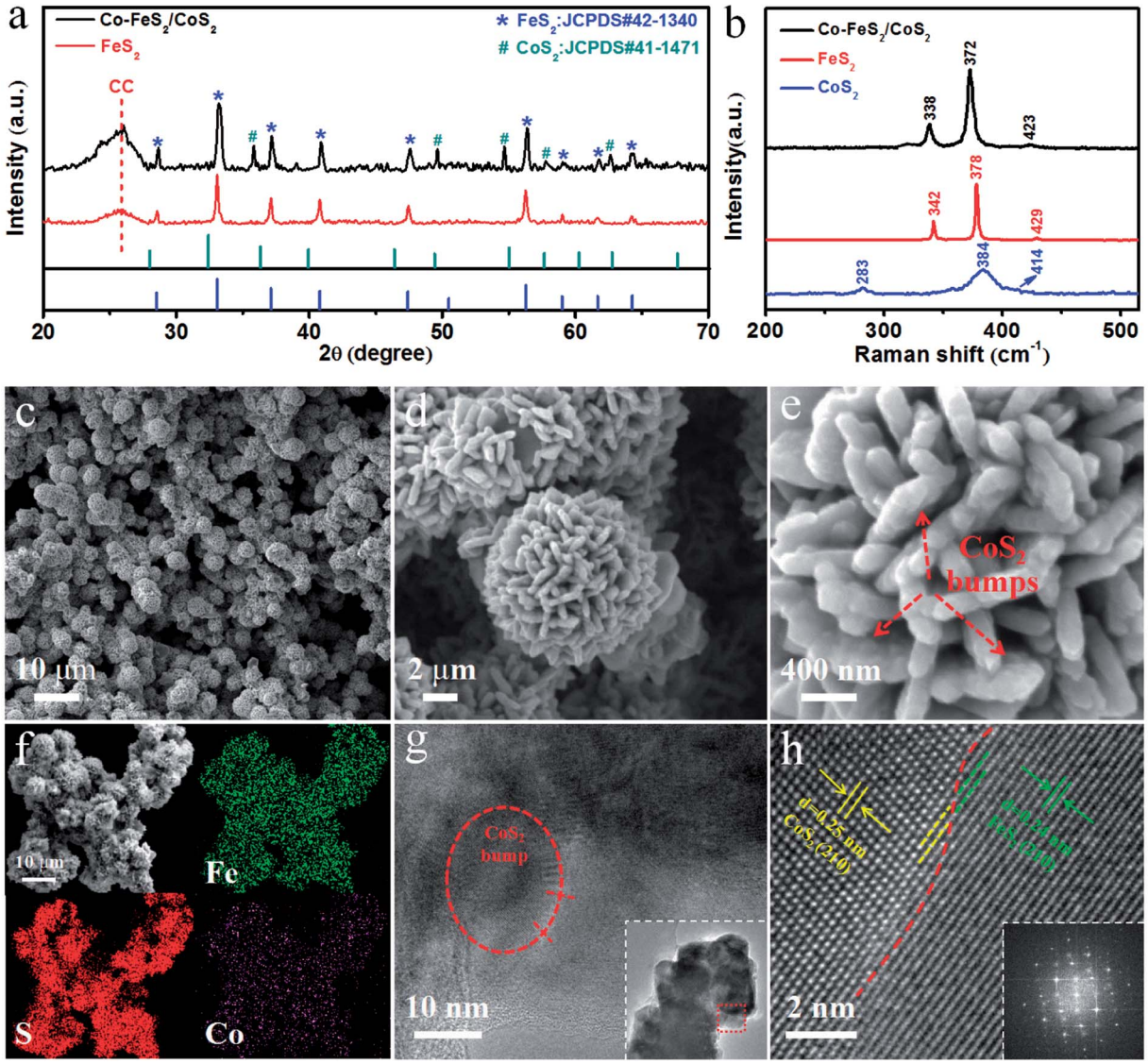

Fig. 1 (a) XRD patterns for Co–FeS_2/CoS_2 and FeS_2; (b) Raman spectra for Co–FeS_2/CoS_2, FeS_2 and CoS_2; (c)–(e) progressively enlarged SEM images of Co–FeS_2/CoS_2; (f) SEM image and corresponding EDX elemental mapping images of Fe, S, Co for Co–FeS_2/CoS_2; (g) TEM image of Co–FeS_2/CoS_2 heterostructures, the inset is TEM image of Co–FeS_2/CoS_2 nanopetals; (h) HRTEM image of Co–FeS_2/CoS_2 heterostructures, the inset is corresponding SAED pattern of Co–FeS_2/CoS_2 heterostructures.

2.2 Synthesis of Co–FeS_2/CoS_2 heterostructures

In this experiment, the carbon cloth (1.8 cm × 2.2 cm) was first ultrasonically clean for 15 minutes using ultrapure water and anhydrous ethanol and then dried. Subsequently, $FeSO_4 \cdot 7H_2O$ (1.2 mM), $Co(NO_3)_2 \cdot 6H_2O$ (0.156 mM), and $SC(NH_2)_2$ (1.8 mM) were added to a 30 mL reaction kettle followed by 25 mL of ultrapure water and stirred for 15 minutes to form a transparent homogeneous solution. Sulfur powder (0.72 mM) was then introduced to the above reactor and stirred at a low speed for 15 minutes. After the stirring was stopped, the magnetic stirrer was removed and sulfur powder film was formed on the liquid surface. The clean and dried carbon cloth was inserted vertically into reaction kettle solution and maintained at 180 °C for 8 hours. After the reactor cooled down to room temperature, the solution was removed, and then samples were washed using ultrapure water and absolute ethanol.

2.3 Materials characterization

The crystal phase properties of the samples were analyzed with a Bruker D8 Advance X-ray diffractometer (XRD) using Cu Kα radiation at 40 kV and 40 mA, for 2θ ranging from 20° to 70°, with a scan rate of 0.1° per second. Raman spectra were obtained by Raman spectroscopy (JY T64000) excited at 514.5 nm of a 100 μW Ar^+ laser. Scanning electron microscopy (FE-SEM; JSM-7000F) was used to obtain the surface morphology of the sample. The energy dispersive spectrometer (EDS; Inca x-stream 034A0) was used to confirm the elemental composition of the sample. Transmission electron microscope (TEM) and high resolution transmission electron microscope (HRTEM) images were obtained by using a JEOL type JEM2100 instrument at an accelerating voltage of 200 kV. The chemical compositions of samples were determined by using X-ray photoelectron spectroscopy (XPS) analysis (PHI5000 Versaprobe).

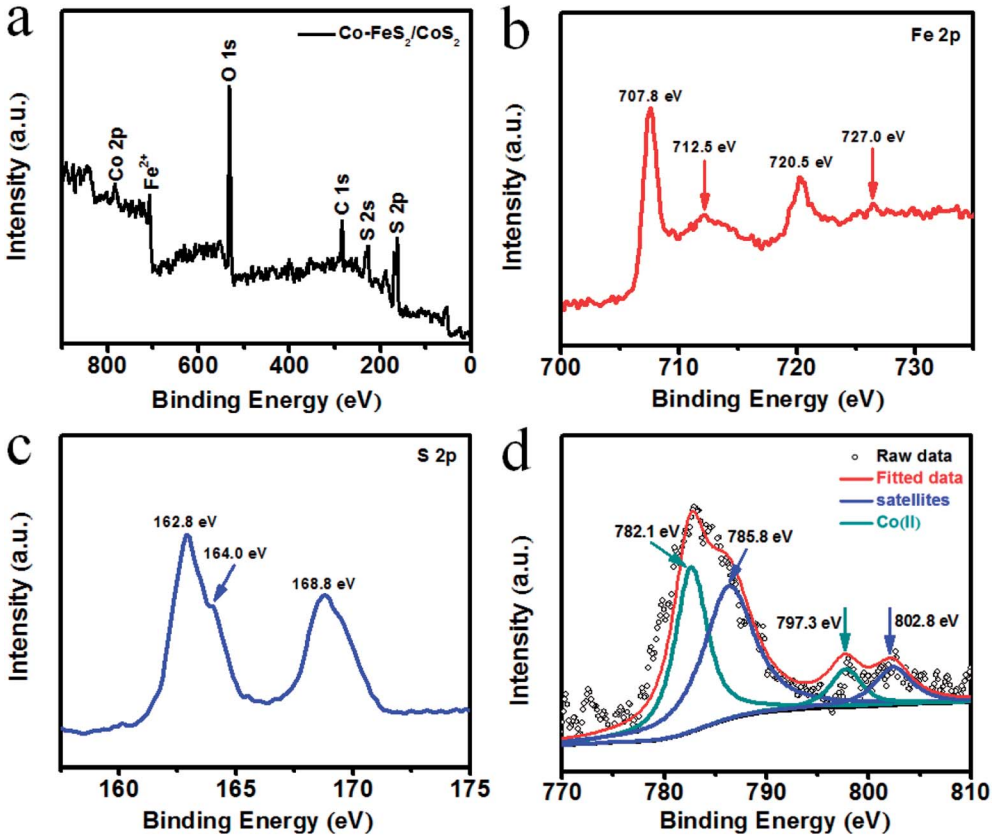

Fig. 2 (a) XPS survey spectrum for Co–FeS_2/CoS_2; XPS spectra of the Co–FeS_2/CoS_2 from (b) Fe 2p, (c) S 2p, (d) Co 2p.

2.4 Electrochemical measurements

Electrochemical measurements were performed with a CHI760E electrochemical analyzer (CH Instruments, Chenhua Co., Shanghai, China). A conventional three-electrode cell was used, including the sample as a working electrode, a calomel electrode as a reference electrode, and a graphite rod as a counter electrode. 1 M KOH and 0.5 M H_2SO_4 solution were used as the electrolyte solution, nitrogen was bubbled into the solution for 30 minutes before testing. In this paper, the positive scan curve is selected as the LSV curve (between 0 and 0.8 V, 2 mV s^{-1}) for OER and the negative scan curve is selected as the LSV curve for HER (between −0.8 and −0.2 V, 2 mV s^{-1}). The Tafel slope is calculated from the logarithmic relationship between overpotential and current density based on the LSV curve. The electrochemical active surface areas (ECSA) were calculated from the double layer charging curves using cyclic voltammograms (CVs) at different scan rates of 2–160 mV s^{-1} in potential range from 0 to 0.20 V *vs.* RHE for HER. Electrochemical impedance spectroscopy (EIS) was performed with a frequency range of 10^5–0.1 Hz. The stability assessment was performed by 1000 cycles of the testing at a scan rate of 100 mV s^{-1}.

3. Results and discussion

In the experiment, we prepared Co–FeS_2/CoS_2 heterostructures with superior electrocatalytic performance through the selection of sulfur sources, regulation of cobalt content, optimization of loading, addition and optimization of dual sulfur sources (as can be seen in ESI†). Fig. 1a shows the X-ray diffraction (XRD) patterns for Co–FeS_2/CoS_2 heterostructures and FeS_2. The peaks at 28.5°, 33.1°, 37.1°, 40.8°, 47.5° and 56.3° can be indexed to the (111), (200), (210), (211), (220), (311) planes of FeS_2 (JCPDS#42-1340).[19,26] The peaks at 35.9°, 49.5°, 54.7°, 57.7° and 62.7° correspond to the planes of (210), (221), (311), (222) and (321) of CoS_2 (JCPDS#41-1471).[8,27] From the XRD pattern, it can be seen that the Co–FeS_2/CoS_2 heterostructures exhibit good crystallinity. Fig. 1b shows the Raman spectra of the Co–FeS_2/CoS_2 heterostructures, FeS_2 and CoS_2. The Raman spectrum for the Co–FeS_2/CoS_2 heterostructures shows a broad primary peak centered around 372 cm^{-1}, which is likely the result of contributions from the most intense FeS_2 peaks at 378 cm^{-1} and the primary CoS_2 peak at 384 cm^{-1}.[28]

As shown in Fig. 1c, Co–FeS_2/CoS_2 exhibits a microflower-like morphology with diameters ranging from 4 to 6 micrometer. Fig. 1d shows the nano-petals structures on the Co–FeS_2/CoS_2 heterostructures, the nano-petals crosslinked together to form a 3D microflower-like structures,[29] which not only increase the specific surface area but also accelerate the outward diffusion rate of the generated gas in the solution for water splitting.[30,31] Fig. 1e is a high-resolution SEM image showing the bumps of CoS_2 on the nano-petals of the Co–FeS_2/CoS_2 heterostructures; Co-doped FeS_2 decreased the kinetic energy barrier of the catalytic reaction, synergistic catalysis by heterostructures of Co–FeS_2/CoS_2 further improves electrocatalytic activity.[10,32–34] Fig. 1f shows the SEM image and the energy-dispersive X-ray

(EDX) spectrum elemental mapping images of Fe, S and Co, for the Co–FeS_2/CoS_2 heterostructures, revealing the distribution of the three elements. Fig. 1g is a TEM image of Co–FeS_2/CoS_2 heterostructures, the inside of the ellipse is a bump of CoS_2 which further increased the surface area of the sample and adjusted the kinetic energy. Fig. 1h is a high resolution TEM (HRTEM) image of Co–FeS_2/CoS_2 heterostructures, the interplanar spacing (210) of FeS_2 is 0.24 nm,[19,35] the interplanar spacings (210) of the CoS_2 bump are 0.25 nm,[36,37] and the inset showed the selected area electron diffraction (SAED) pattern, which shows the monocrystallinity of the sample. All these potentially explain the excellent electrocatalytic performance of the Co–FeS_2/CoS_2 heterostructures.

Fig. 2a presents the full XPS survey spectrum of the Co–FeS_2/CoS_2 heterostructures, also confirming the presence of Fe, S and Co elements. Fig. 2b shows the XPS spectrum of Fe (2p); the characteristic peaks of Co–FeS_2/CoS_2 were detected at 707.8 (Fe $2p_{3/2}$) and 720.5 eV (Fe $2p_{1/2}$) due to the Fe^{2+} of the FeS_2 structure.[7] The peaks at 712.5 and 727.0 eV can be attributed to a small amount of Fe^{2+} being oxidized to Fe^{3+}.[38] The XPS spectra of Co–FeS_2/CoS_2 were measured in the S (2p) region, as shown in Fig. 2c. The binding energies of S (2p) at 162.8 and 164.0 eV belong to S_2^{2-} of FeS_2.[39,40] There were some oxidized S species found (168.8 eV) in Co–FeS_2/CoS_2.[41,42] As shown in Fig. 2d, the Co 2p spectrum can be deconvoluted into four peaks: the Co $2p_{3/2}$ and Co $2p_{1/2}$ peaks at 782.1 and 797.3 eV can be attributed to Co^{2+} bound to oxygen,[43,44] while another two peaks at 785.8 and 802.8 eV are ascribed to higher oxidized cobalt species (Co^{3+}).[45]

We further analyzed the main process of formation of Co–FeS_2/CoS_2 heterostructures. We speculate the following reaction process: solid sulfur powder attached to the carbon cloth at 180 °C is melted into small droplets. At the sulfur powder droplets and solution interface, due to the severe excess in sulfur powder compared to Fe^{2+}, Co^{2+}, and S^{2-}. Co^{2+} was incorporated into the reaction of Fe^{2+}, S^{2-}, and sulfur powder droplets (S^0). When Co–FeS_2 was formed, Co^{2+} further reacted with sulfur powder droplets (S^0)/S^{2-} to form CoS_2, thus forming the Co–FeS_2/CoS_2 heterostructures.

To our knowledge, Co–FeS_2/CoS_2 heterostructures has not yet been explored for the electrocatalytic splitting of water into hydrogen and oxygen. Unique 3D hierarchical nanostructures not only increase the surface area but also facilitates the release of hydrogen and oxygen from the electrode surface. The superior oxygen evolution performance of the Co–FeS_2/CoS_2 heterostructures were mainly attributed to the presence of the CoS_2 phase and the formation of heterostructures with the Co–FeS_2.[46] In addition, density functional theory calculation revealed that sulfur was responsible for the active sites for proton adsorption and reduction; the high catalytic activity was stemmed from a large reduction of the kinetic energy barrier of H atom adsorption on FeS_2 surface upon Co doping in the iron pyrite structure.[18,19] The formation of heterostructures for Co–FeS_2 and CoS_2 further lowers the kinetic

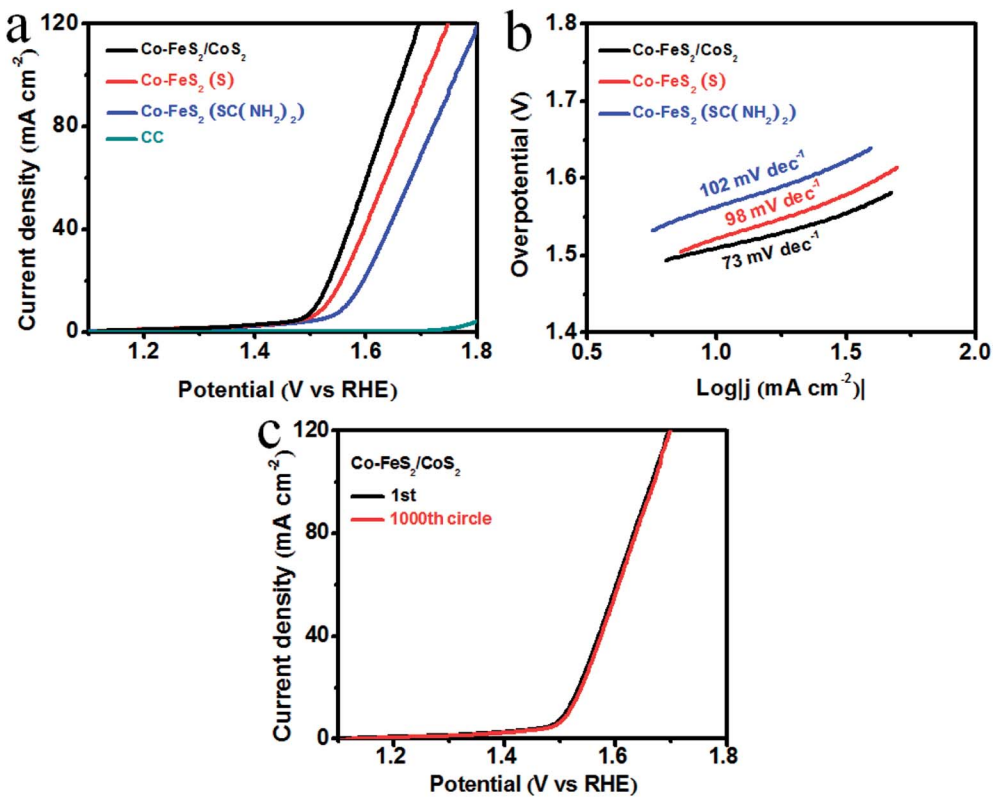

Fig. 3 (a) LSV curves of Co–FeS_2/CoS_2, Co–FeS_2 (S), Co–FeS_2 ($SC(NH_2)_2$), and bare CC for OER in 1 M KOH solution; (b) corresponding Tafel plots; (c) LSV curves of Co–FeS_2/CoS_2 before and after 1000 CV cycles.

energy barrier of the reaction to gain superior electrocatalytic performance.[23–25]

We used a typical three-electrode system with a sweeping rate of 2 mV s^{-1} to test the OER electrocatalytic activity and stability of the Co–FeS_2/CoS_2 heterostructures. For comparison study, the electrocatalytic activity of Co–FeS_2 synthesized using sulfur powder or thiourea was also tested. Fig. 3a shows the linear sweep voltammetry (LSV) curves, showing that bare CC almost has no OER activity. Co–FeS_2/CoS_2 heterostructures shows superior OER activity, with an overpotential of only 278 mV required to drive 10 mA cm^{-2}. This is better than the overpotential of 292 mV for Co–FeS_2 (S) and 333 mV for Co–FeS_2 ($SC(NH_2)_2$). Fig. 3b shows that the Tafel slope of Co–FeS_2/CoS_2 is 73 mV dec^{-1}, which is superior to the measured 98 mV dec^{-1} of Co–FeS_2 (S) and 102 mV dec^{-1} of Co–FeS_2 ($SC(NH_2)_2$). As shown in Fig. 3c, the overpotential of Co–FeS_2/CoS_2 is only 283 mV after 1000 cycles, which signifies Co–FeS_2/CoS_2 heterostructures have good electrochemical stability in strongly alkaline solutions.

HER activity was analyzed by measuring the LSV curves of Co–FeS_2/CoS_2 and bare CC in 0.5 M H_2SO_4 solution. In the polarization curve of Fig. 4a, the blank substrate of CC shows negligible HER activity over the measured voltage range, indicating that the HER performance of the CC has little contribution. The Co–FeS_2/CoS_2 heterostructures grown on the CC substrate achieved geometric current densities of −10 mA cm^{-2} at much lower overpotential of −103 mV *versus* the reversible hydrogen electrode (RHE) compared to that of Co–FeS_2 (−161 mV for (S) and −173 mV for $SC(NH_2)_2$). As shown in Fig. 4b, Co–FeS_2/CoS_2 heterostructures have a Tafel slope of 56 mV dec^{-1}, smaller than those for Co–FeS_2 70 mV dec^{-1} for (S) and 68 mV dec^{-1} for $SC(NH_2)_2$. To investigate the origin of the superior activity of Co–FeS_2/CoS_2 heterostructures, we further estimated the ECSA by calculating its non-faradaic double-layer capacitance using cyclic voltammetry measurement, since ECSA value is linearly proportional to C_{dl}.[46–48] As shown in Fig. S10a–d,† cyclic voltammograms were measured in the non-faradaic capacitance current range, the C_{dl} value of hierarchical Co–FeS_2/CoS_2 is 86 mF cm^{-2} is larger than that of Co–FeS_2(S) (37 mF cm^{-2}) and Co–FeS_2($SC(NH_2)_2$) (20 mF cm^{-2}). The result indicates that hierarchical architecture and bump feature can maximize the exposure of accessible active sites, which contributes to excellent electrocatalytic performance of Co–FeS_2/CoS_2 heterostructures. In addition, as shown in Fig. S10e,† the reaction kinetics is verified by EIS, the hierarchical Co–FeS_2/CoS_2 heterostructures present a smaller semicircle than Co–FeS_2(S) and Co–FeS_2($SC(NH_2)_2$), which can be associated with interfacial charge transfer process, a lower value corresponds to a faster electron transfer rate. This result demonstrated further the faster catalytic kinetics of Co–FeS_2/CoS_2 heterostructures.[49–51] In addition to catalytic activity, stability is another critical factor to evaluate a good electrocatalyst, we investigated the stability of Co–FeS_2/CoS_2 heterostructures *via* 1000 cycles scanning. As shown in Fig. 4c, the Co–FeS_2/CoS_2 electrode lost only 3 mV of overpotential at −10 mV cm^{-2} after

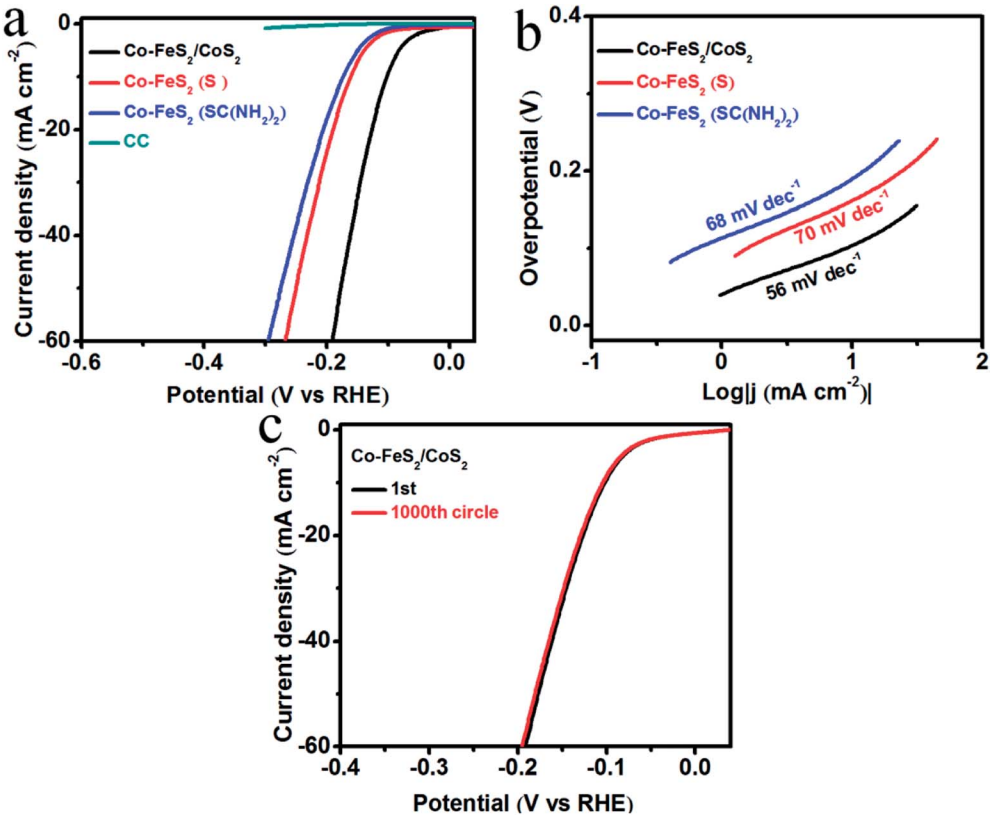

Fig. 4 (a) LSV curves of Co–FeS_2/CoS_2, Co–FeS_2/CoS_2 (S), Co–FeS_2 ($SC(NH_2)_2$), and bare CC for HER in 0.5 M H_2SO_4 solution; (b) corresponding Tafel plots; (c) LSV curves of Co–FeS_2/CoS_2 before and after 1000 cycles.

Table 1 Summary of HER and OER activity of electrocatalysts

Catalyst	Electrolyte	η_j (mV *vs.* RHE)	Tafel slope (mV dec^{-1})	η_j (mV *vs.* OER)	Reference
FeS_2	0.1 M KOH	$\eta_{-10} = -96$	78	—	19
FeS_2	0.5 M H_2SO_4	$\eta_{-10} = -139$	66	—	7
$Fe_{0.68}Co_{0.32}S_2$	0.5 M H_2SO_4	$\eta_{-10} = -166$	51	—	38
CoS_2	0.5 M H_2SO_4	$\eta_{-10} = -145$	51.6	—	8
CoS_2	0.5 M H_2SO_4	$\eta_{-100} = -140$	70.1	—	27
CoS_2	0.1 M KOH	—	—	$\eta_{10} = 290$	52
Co–FeS_2/CoS_2	**0.5 M H_2SO_4**	$\boldsymbol{\eta_{-10} = -103}$	**56**	$\boldsymbol{\eta_{10} = 278}$	**This work**

1000 cycles. Furthermore, we analyzed the characterization results of the Co–FeS_2/CoS_2 heterostructures before and after the 1000 cycles. As shown in Fig. S11,† it was found that the XRD patterns, XPS spectra, SEM, and TEM images of Co–FeS_2/CoS_2 heterostructures did not significantly changed. The Co–FeS_2/CoS_2 heterostructures also has excellent electrochemical stability in 0.5 M H_2SO_4 solution, which is better than the previously reported non-noble metal-based sulfide electrocatalyst, presented in Table 1.

4. Conclusions

In summary, by optimizing experiment conditions, Co–FeS_2/CoS_2 heterostructures were successfully prepared by the hydrothermal route with excellent OER and HER electrocatalytic performance. Their unique three-dimensional structure not only increases the surface area but also facilitates the release of hydrogen and oxygen from the electrode surface. Co-doped FeS_2 and CoS_2 formed heterostructures on the petals of Co–FeS_2, which change the energy barrier of the catalytic reaction to gain excellent electrocatalytic performance. This study not only provides a low-cost, stable and earth-abundant iron-based electrocatalyst for efficient water splitting, it will also provide an exciting new method for the rational design and scalable preparation of three-dimensional polynary heterostructures as electrocatalysts.

Conflicts of interest

There are no conflicts to declare.

Acknowledgements

This work was financially supported by the National Basic Research Program of China (2018YFA0209101), the National Science Foundations of China (No. 61205057, No. 11574136), Qing Lan Project, the '1311 Talent Plan' Foundation of Nanjing University of Posts and Telecommunications, Six Talent Peaks Project in Jiangsu Province (JY-014), and State Key Laboratory of High Performance Computing, National University of Defense Technology.

References

1 C. Tang, L. Gan, R. Zhang, W. Lu, X. Jiang and A. M. Asiri, Ternary $Fe_xCo_{1-x}P$ nanowire array as a robust hydrogen evolution reaction electrocatalyst with pt-like activity: experimental and theoretical insight, *Nano Lett.*, 2016, **16**, 6617–6621.

2 W. Xiong, Z. Guo, H. Li, R. Zhao and X. Wang, Rational bottom-up engineering of electrocatalysts by atomic layer deposition: a case study of $Fe_xCo_{1-x}S_y$-based catalysts for electrochemical hydrogen evolution, *ACS Energy Lett.*, 2017, **2**, 2778–2785.

3 X. Zou and Y. Zhang, Noble metal-free hydrogen evolution catalysts for water splitting, *Chem. Soc. Rev.*, 2015, **44**, 5148–5180.

4 J. Wang, W. Cui, Q. Liu, Z. Xing, A. M. Asiri and X. Sun, Recent progress in cobalt-based heterogeneous catalysts for electrochemical water splitting, *Adv. Mater.*, 2016, **28**, 215–230.

5 Y. Li, H. Zhang, M. Jiang, Q. Zhang, P. He and X. Sun, 3D self-supported Fe-doped Ni_2P nanosheet arrays as bifunctional catalysts for overall water splitting, *Adv. Funct. Mater.*, 2017, **27**, 1702513.

6 X. Yu, Y. Feng, Y. Jeon, B. Guan, X. W. Lou and U. Paik, Formation of Ni-Co-MoS_2 nanoboxes with enhanced electrocatalytic activity for hydrogen evolution, *Adv. Mater.*, 2016, **28**, 9006–9011.

7 Y. Chen, S. Xu, Y. Li, R. J. Jacob, Y. Kuang and B. Liu, FeS_2 Nanoparticles embedded in reduced graphene oxide toward robust, high-performance electrocatalysts, *Adv. Energy Mater.*, 2017, **7**, 1700482.

8 M. S. Faber, R. Dziedzic, M. A. Lukowski, N. S. Kaiser, Q. Ding and S. Jin, High-performance electrocatalysis using metallic cobalt pyrite (CoS_2) micro-and nanostructures, *J. Am. Chem. Soc.*, 2014, **136**, 10053–10061.

9 Y. Wang, B. Kong and D. Zhao, Strategies for developing transition metal phosphides as heterogeneous electrocatalysts for water splitting, *Nano Today*, 2017, **15**, 26–55.

10 X. Q. Lu, X. Yan and S. Devaramani, Self-supported rectangular CoP nanosheet arrays grown on carbon cloth as an efficient electrocatalysts for hydrogen evolution reaction over a variety of pH values 1, *New J. Chem.*, 2017, **41**, 2436–2442.

11 C. Ouyang, X. Wang and S. Wang, Phosphorus-doped CoS_2 nanosheet arrays as ultra-efficient electrocatalysts for the hydrogen evolution reaction, *Chem. Commun.*, 2015, **51**, 14160–14163.

12 D. Wang, D. Zhang, C. Tang, P. Zhou and Z. Wu, Hydrogen evolution catalyzed by cobalt promoted molybdenum phosphide nanoparticles, *Catal. Sci. Technol.*, 2016, **6**, 1952–1956.

13 X. Zhu, T. Jin, C. Tian, C. Lu, X. Liu and M. Zeng, *In situ* coupling strategy for the preparation of FeCo alloys and Co_4N hybrid for highly efficient oxygen evolution, *Adv. Mater.*, 2017, **29**, 1704091.

14 W. Fang, D. Liu, Q. Lu, X. Sun and A. M. Asiri, Nickel promoted cobalt disulfide nanowire array supported on carbon cloth: an efficient and stable bifunctional electrocatalyst for full water splitting, *Electrochem. Commun.*, 2016, **63**, 60–64.

15 V. Bachvarov, E. Lefterova and R. Rashkov, Electrodeposited NiFeCo and NiFeCoP alloy cathodes for hydrogen evolution reaction in alkaline medium, *Int. J. Hydrogen Energy*, 2016, **41**, 12762–12771.

16 X. Zhang, X. Zhang, H. Xu, Z. Wu, H. Wang and Y. Liang, Iron-doped cobalt monophosphide nanosheet/carbon nanotube hybrids as active and stable electrocatalysts for water splitting, *Adv. Funct. Mater.*, 2017, **27**, 1606635.

17 X. P. Han, X. Y. Wu, C. Zhong and Y. d. Deng, $NiCo_2S_4$, nanocrystals anchored on nitrogen-doped carbon nanotubes as a highly efficient bifunctional electrocatalyst for rechargeable zinc-air batteries, *Nano Energy*, 2017, **31**, 541–550.

18 D. Y. Wang, M. Gong and H. L. Chou, Highly active and stable hybrid catalyst of cobalt-doped FeS_2 nanosheets-carbon nanotubes for hydrogen evolution reaction, *J. Am. Chem. Soc.*, 2015, **137**, 1587–1592.

19 R. Miao, B. Dutta, S. Sahoo, J. He, W. Zhong and S. A. Cetegen, Mesoporous iron sulfide for highly efficient electrocatalytic hydrogen evolution, *J. Am. Chem. Soc.*, 2017, **139**, 13604–13607.

20 J. Yu, G. Cheng and W. Luo, Ternary nickel–iron sulfide microflowers as a robust electrocatalyst for bifunctional water splitting, *J. Mater. Chem. A*, 2017, **5**, 15838–15844.

21 Z. Wu, X. Wang, J. Huang and F. Gao, A Co-doped Ni–Fe mixed oxide mesoporous nanosheet array with low overpotential and high stability towards overall water splitting, *J. Mater. Chem. A*, 2018, **6**, 167–178.

22 K. Ao, D. Li and Y. Yao, Fe-doped Co_9S_8, nanosheets on carbon fiber cloth as pH-universal freestanding electrocatalysts for efficient hydrogen evolution, *Electrochim. Acta*, 2018, **264**, 157–165.

23 T. Kuo, W. Chen and H. Liao, Improving hydrogen evolution activity of earth-abundant cobalt-doped iron pyrite catalysts by surface modification with phosphide, *Small*, 2017, **13**, 1603356.

24 C. Zhu, A. L. Wang, W. Xiao, D. Chao and X. Zhang, *In situ* grown epitaxial heterojunction exhibits high-performance electrocatalytic water splitting, *Adv. Mater.*, 2018, **30**, 1705516.

25 P. Ganesan, A. Sivanantham and S. Shanmugam, CoS_2-TiO_2 hybrid nanostructures: efficient and durable bifunctional electrocatalysts for alkaline electrolyte membrane water electrolyzers, *J. Mater. Chem. A.*, 2018, 1075–1085.

26 L. Xu, Y. Hu and H. Zhang, Confined synthesis of FeS_2 nanoparticles encapsulated in carbon nanotube hybrids for ultrastable lithium-ion batteries, *ACS Sustainable Chem. Eng.*, 2016, **4**, 4251–4255.

27 H. Zhang, Y. Li, G. Zhang, T. Xu, P. Wan and X. Sun, A metallic CoS_2 nanopyramid array grown on 3D carbon fiber paper as an excellent electrocatalyst for hydrogen evolution, *J. Mater. Chem. A*, 2015, **3**, 6306–6310.

28 M. S. Faber, M. A. Lukowski, Q. Ding, N. S. Kaiser and S. Jin, Earth-abundant metal pyrites (FeS_2, CoS_2, NiS_2, and their Alloys) for highly efficient hydrogen evolution and polysulfide reduction electrocatalysis, *J. Phys. Chem. C*, 2014, **118**, 21347–21356.

29 Z. Z. Wu, C. Y. Tang, P. Zhou and Z. H. Liu, Enhanced hydrogen evolution catalysis from osmotic swelled ammoniated MoS_2, *J. Mater. Chem. A*, 2015, **3**, 13050–13056.

30 J. Yu, G. Cheng and W. Luo, Hierarchical NiFeP microflowers directly grown on Ni foam for efficient electrocatalytic oxygen evolution, *J. Mater. Chem. A*, 2017, **5**, 11229–11235.

31 X. Y. Wu, X. P. Han, X. Y. Ma and W. Zhang, Morphology-Controllable Synthesis of Zn-Co-Mixed Sulfide Nanostructures on Carbon Fiber Paper Toward Efficient Rechargeable Zinc–Air Batteries and Water Electrolysis, *ACS Appl. Mater. Interfaces*, 2017, **9**, 12574–12583.

32 H. Zhang, X. Li, A. Hähnel, V. Naumann, C. Lin and S. Azimi, Bifunctional heterostructure assembly of NiFe LDH nanosheets on NiCoP nanowires for highly efficient and stable overall water splitting, *Adv. Funct. Mater.*, 2018, **28**, 1706847.

33 H. Song, S. Oh, H. Yoon, K. H. Kim, S. Ryu and J. Oh, Bifunctional NiFe inverse opal electrocatalysts with heterojunction Si solar cells for 9.54%-efficient unassisted solar water splitting, *Nano Energy*, 2017, **42**, 1–7.

34 H. Yu, Y. Xue, L. Hui, C. Zhang, Y. Li and Z. Zuo, Efficient hydrogen production on a 3D flexible heterojunction material, *Adv. Mater.*, 2018, 1707082.

35 L. Zhu, B. J. Richardson and Q. Yu, Anisotropic growth of iron pyrite FeS_2 nanocrystals *via* oriented attachment, *Chem. Mater.*, 2015, **27**, 150427111020001.

36 Y. Guo, L. Gan and C. Shang, A cake-style CoS_2@MoS_2/RGO hybrid catalyst for efficient hydrogen evolution, *Adv. Funct. Mater.*, 2017, **27**, 1602699.

37 H. Zhang, Y. Li and G. Zhang, Highly crystallized cubic cattierite CoS_2, for electrochemically hydrogen evolution over wide pH range from 0 to 14, *Electrochim. Acta*, 2014, **148**, 170–174.

38 S. Y. Huang, D. Sodano, T. Leonard, S. Luiso and P. S. Fedkiw, Cobalt-doped iron sulfide as an electrocatalyst for hydrogen evolution, *J. Electrochem. Soc.*, 2017, **164**, 276–282.

39 M. Zheng, Y. Ding, L. Yu, X. Du and Y. Zhao, *In situ* grown pristine cobalt sulfide as bifunctional photocatalyst for hydrogen and oxygen evolution, *Adv. Funct. Mater.*, 2017, **27**, 1605846.

40 X. Y. Ma, W. Zhang, Y. D. Deng and C. Zhong, Phase and composition controlled synthesis of cobalt sulfide hollow

nanospheres for electrocatalytic water splitting, *Nanoscale*, 2018, **10**, 4816–4824.

41 L. Fang, Y. Zhang, Y. Guan, H. Zhang, S. Wang and Y. Wang, Specific synthesis of CoS_2 nanoparticles embedded in porous Al_2O_3 nanosheets for efficient hydrogen evolution and enhanced lithium storage, *J. Mater. Chem. A*, 2017, **5**, 2861–2869.

42 J. Jiang, S. Lu, H. Gao, X. Zhang and H. Q. Yu, Ternary $FeNiS_2$ ultrathin nanosheets as an electrocatalyst for both oxygen evolution and reduction reactions, *Nano Energy*, 2016, **27**, 526–534.

43 R. Zhang, X. Wang and S. Yu, Ternary $NiCo_2Px$ nanowires as pH-universal electrocatalysts for highly efficient hydrogen evolution reaction, *Adv. Mater.*, 2016, **29**, 1605502.

44 M. Nakayama, F. Kotaro and T. Kobayakawa, A binder-free thin film anode composed of Co^{2+}-intercalated buserite grown on carbon cloth for oxygen evolution reaction, *Electrochem. Commun.*, 2017, **84**, 24–27.

45 M. Ma, G. Zhu, F. Xie, F. Qu, Z. Liu and G. Du, Homologous catalysts based on Fe-doped CoP nanoarrays for high-performance full water splitting under benign conditions, *ChemSusChem*, 2017, **10**, 3188–3192.

46 Y. Hua, H. Jiang and H. Jiang, Hierarchical porous CoS_2 microboxes for efficient oxygen evolution reaction, *Electrochim. Acta*, 2018, **278**, 219–225.

47 S. Hao, L. Yang and D. Liu, Integrating natural biomass electro-oxidation and hydrogen evolution: using a porous Fe-doped CoP nanosheet array as a bifunctional catalyst, *Chem. Commun.*, 2017, **53**, 5710–5713.

48 Y. Wang, Y. Ni and B. Liu, Vertically oriented CoO@FeOOH nanowire arrays anchored on carbon cloth as a highly efficient electrode for oxygen evolution reaction, *Electrochim. Acta*, 2017, **257**, 356–363.

49 X. Wang, F. Li and W. Li, Hollow bimetallic cobalt-based selenide polyhedrons derived from metal-organic framework: an efficient bifunctional electrocatalyst for overall water splitting, *J. Mater. Chem. A*, 2017, 17982–17989.

50 Y. Teng, X. D. Wang and H. Y. Chen, Iron-assisted engineering of molybdenum phosphide nanowires on carbon cloth for efficient hydrogen evolution in a wide pH range, *J. Mater. Chem. A*, 2017, 22790–22796.

51 Z. Gao, Q. Gao and Z. Liu, High-efficiency hydrogen evolution catalyzed by iron phosphide nanocrystals, *RSC Adv.*, 2016, **6**, 114430–114435.

52 J. Yang, Z. Yang and L. H. Li, Highly efficient oxygen evolution from CoS_2/CNT nanocomposites *via* a one-step electrochemical deposition and dissolution method, *Nanoscale*, 2017, **9**, 6886–6894.